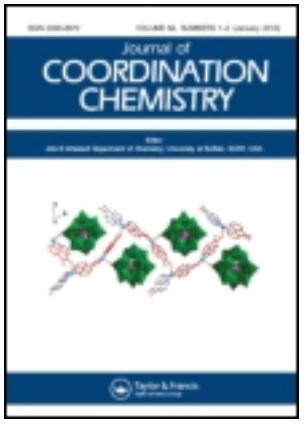

Journal of Coordination Chemistry
Publication details, including instructions for authors and subscription information:
http://www.tandfonline.com/loi/gcoo20

Coordination polymers of Cu^{II} and Ni^{II} with 3-pyridin-3-yl-benzoate: crystal structures and magnetic properties

Long Tang [a], Feng Fu [a], Yapan Wu [a], Xiangyang Hou [a] & Loujun Gao [a]

[a] Department of Chemistry and Chemical Engineering, Shaanxi Key Laboratory of Chemical Reaction Engineering, Yan'an University, Yan'an, Shaanxi 716000, China

Published online: 09 Sep 2011.

To cite this article: Long Tang, Feng Fu, Yapan Wu, Xiangyang Hou & Loujun Gao (2011) Coordination polymers of Cu^{II} and Ni^{II} with 3-pyridin-3-yl-benzoate: crystal structures and magnetic properties, Journal of Coordination Chemistry, 64:18, 3136-3145, DOI: 10.1080/00958972.2011.614347

To link to this article: http://dx.doi.org/10.1080/00958972.2011.614347

Journal of Coordination Chemistry
Vol. 64, No. 18, 20 September 2011, 3136–3145

Coordination polymers of Cu^{II} and Ni^{II} with 3-pyridin-3-yl-benzoate: crystal structures and magnetic properties

LONG TANG, FENG FU*, YAPAN WU, XIANGYANG HOU and LOUJUN GAO

Department of Chemistry and Chemical Engineering, Shaanxi Key Laboratory of Chemical Reaction Engineering, Yan'an University, Yan'an, Shaanxi 716000, China

(*Received 10 May 2011; in final form 25 July 2011*)

Coordination polymers of Cu^{II} and Ni^{II} with 3-pyridin-3-yl-benzoic acid (3,3-Hpybz), $\{[Cu(3,3\text{-pybz})_2(CH_3OH)]\cdot(DMF)\}_n$ (**1**) and $\{[Ni(3,3\text{-pybz})_2(H_2O)]\cdot(H_2O)\}_n$ (**2**), were synthesized and characterized by single-crystal X-ray diffraction, thermogravimetric analyses, elemental analysis, and IR spectroscopy. In **1**, Cu^{II} ions are linked by paired 3,3-pybz ligands to generate an infinite 1-D double-strand chain. However, Ni^{II} ions in **2** are linked by the 3,3-pybz to form a 2-D corrugated network with a simple (4,4) topology; these 2-D layers are further enlarged to form the final 3-D supramolecular edifice *via* strong aromatic π–π stacking interactions and O–H···O hydrogen bonds. Magnetic properties of **1** and **2** have also been investigated.

Keywords: Coordination polymer; Magnetic properties; Cobalt(II); Nickel(II)

1. Introduction

Coordination polymers based on multifunctional organic ligands and metal ions have attracted attention for topologies and potential applications in catalysis, molecular recognition, and photochemistry [1–4]. Effective strategy to construct these coordination polymers is to select suitable multifunctional ligands to integrate metal ions to a desired framework [5, 6]. Multidentate bridging ligands containing functional groups such as pyridyl and/or carboxylate have proven to be among the most important types of organic ligands for coordination polymers exhibiting remarkable polymeric structural motifs due to their rich coordination modes [7–10].

Pyridine carboxylic acids, as multidentate bridging ligands, containing N- or/and O-donors have been used widely. In our previous work, several compounds with pyridine carboxylic acids have been reported [11–15]. To continue our research, we have investigated the coordination chemistry of the 3-pyridin-3-yl-benzoic acid (3,3-Hpybz), and some complexes with 3,3-Hpybz have been reported [16, 17]. Herein, we report the syntheses and characterizations of two new M(II) coordination complexes,

*Corresponding author. Email: yadxgncl@126.com

Journal of Coordination Chemistry
ISSN 0095-8972 print/ISSN 1029-0389 online
DOI: 10.1080/00958972.2011.614347

$\{[Cu(3,3\text{-pybz})_2(CH_3OH)]\cdot(DMF)\}_n$ (**1**) and $\{[Ni(3,3\text{-pybz})_2(H_2O)]\cdot(H_2O)\}_n$ (**2**). The magnetic properties of **1** and **2** have also been investigated.

2. Experimental

2.1. *Materials and methods*

Commercially available solvents and starting materials were used as received. C, H, and N microanalyses were carried out with an Elementar Vario EL III elemental analyzer. FT-IR spectra were recorded from KBr pellets from 4000 to 400 cm^{-1} on a Bruker EQUINOX-55 spectrometer. Thermogravimetric analyses (TGA) were performed under air with a heating rate of 10°C min^{-1} using a NETZSCH STA 449C thermogravimetric analyzer. Magnetic susceptibilities were obtained on crystalline samples using a Quantum Design MPMS SQUID magnetometer; experimental susceptibilities were corrected for the sample holder; and the diamagnetism contributions were estimated from Pascal's constants.

2.2. *Synthesis of $\{[Cu(3,3\text{-pybz})_2(CH_3OH)]\cdot(DMF)\}_n$ (1)*

A solution of 3-pyridin-3-yl-benzoic acid (0.1 mmol) in N,N-dimethyl formamide (DMF) (5 mL) was placed at the bottom of a straight glass tube, over which a solution of $Cu(NO_3)\cdot 3H_2O$ (0.1 mmol) in methanol (5 mL) was carefully layered. Over a period of 2 weeks, blue block single crystals were obtained (yield: 53% based on Cu). Elemental analysis calcd for $C_{28}H_{27}N_3O_6Cu$ (%): C, 59.51; H, 4.82; N, 7.44. Found (%): C, 59.45; H, 4.68; N, 7.39. IR data (KBr cm^{-1}): 3442(s), 3086(s), 1972(w), 1602(s), 1546(vs), 1421(s), 1380(vs), 1335(s), 1257(w), 1138(m), 1059(m), 1027(w), 876(m), 769(m), 721(w), 678(m), 567(m).

2.3. *Synthesis of $\{[Ni(3,3\text{-pybz})_2(H_2O)]\cdot(H_2O)\}_n$ (2)*

An aqueous solution (10 mL) containing 3-pyridin-3-yl-benzoic acid (0.10 mmol) and $Ni(NO_3)_2\cdot 6H_2O$ (0.10 mmol) was placed in a Parr Teflon-lined stainless steel vessel (25 mL) under autogenous pressure and heated to 160°C for 5d, subsequently cooled to room temperature at a rate of 5°C h^{-}. Green block crystalline products were obtained (yield: 56% based on Ni). Elemental analysis calcd for $C_{24}H_{20}N_2O_6Ni$ (%): C, 58.69; H, 4.10; N, 5.70. Found (%): C, 58.56; H, 3.86; N, 5.57%. IR (KBr pellet, cm^{-1}): 3384(b), 3062(w), 2976(w), 1933(w), 1837(w), 1626(s), 1546(s), 1434(vs), 1411(s), 1388(vs), 1192(m), 1038(m), 806(m), 776(vs), 704(vs), 678(m).

2.4. *Crystal structure determination*

Single-crystal X-ray diffraction (XRD) data for **1** and **2** were collected on a Bruker SMART 1000 CCD diffractometer employing graphite-monochromated Mo-Kα radiation ($\lambda = 0.71073$ Å). The structures were solved by direct methods and refined by full-matrix least-squares on F^2 using SHELXS 97 and SHELXL 97 programs,

Table 1. Crystal data and structure refinement for **1** and **2**.

Empirical formula	$C_{28}H_{27}CuN_3O_6$	$C_{24}H_{20}N_2O_6Ni$
Formula weight	565.07	491.12
Temperature (K)	296(2)	273(2)
Crystal system	Orthorhombic	Monoclinic
Space group	$Pna2_1$	$P2(1)/c$
Unit cell dimensions (Å, °)		
a	16.486(4)	10.4720(7)
b	8.3687(17)	12.8992(9)
c	18.599(4)	16.0309(11)
α	90	90
β	90	95.958(10)
γ	90	90
Volume (Å^3), Z	2566.1(9), 4	2153.8(3), 4
Calculated density (g cm^{-3})	1.463	1.515
Absorption coefficient (mm^{-1})	0.900	0.946
$F(000)$	1172	1016
θ range for data collection (°)	2.19–25.10	1.96–25.05
Index range	$19 \le h \le 16$; $-9 \le k \le 7$; $-22 \le l \le 22$	$-12 \le h \le 12$; $-11 \le k \le 15$; $-19 \le l \le 18$
Reflections collected/unique	12,470/4429 [R(int) = 0.0258]	11,128/3812 [R(int) = 0.0205]
Data/restraints/parameters	4429/2/350	3812/4/298
Goodness-of-fit on F^2	1.035	1.038
Final R_1, wR_2 [$I > 2\sigma(I)$][a]	0.0263, 0.0664	0.0283, 0.0699
R_1, wR_2 (all data)	0.0300, 0.0685	0.0347, 0.0735

[a] $R = \Sigma||F_o| - |F_c||/\Sigma|F_o|$ and $wR_2 = [\Sigma[w(F_o^2 - F_c^2)^2]/\Sigma[(F_o^2)^2]]^{1/2}$.

respectively [18, 19]. Non-hydrogen atoms were refined anisotropically and hydrogen atoms were placed in geometrically calculated positions. The crystallographic data for **1** and **2** are listed in table 1, and selected bond lengths and angles are listed in table 2.

3. Results and discussion

3.1. *Crystal structure*

3.1.1. Structure of $\{[Cu(3,3\text{-pybz})_2(CH_3OH)]\cdot(DMF)\}_n$ (1). Single crystal XRD analysis suggests that the asymmetric unit of **1** consists of one Cu^{II}, two 3,3-pybz anions, one methanol and one free DMF. Each Cu^{II} is five-coordinate with two pyridyl nitrogen atoms and two carboxylate oxygen atoms from four 3,3-pybz anions as well as one oxygen atom from methanol, forming a distorted CuO_3N_2 square-pyramidal geometry with one methanol-O occupying the apex (figure 1). In **1**, the two sets of Cu–N bonds are comparable (2.027(2) and 2.035(2) Å) and the equatorial Cu–O lengths of 1.9480(17) and 1.9782(16) Å are significantly shorter than that of the apical Cu–O5 (2.307(2) Å) bond due to Jahn–Teller distortion; the Cu^{II} deviates from the basal plane by 0.200 Å. The O/N–Cu–O/N bond angles are 87.25(8)° and 173.65(7)°. In this structure, 3,3-pybz adopts μ_2-unidentate (N_{py})/unidentate(O_{COO^-}) coordination (μ_2-κ_1-N:κ_1-O see **s**cheme 1A in the Supplementary material). The dihedral angles are 32.75° (μ_2-κ_1-N:κ_1-O) between pyridine and phenyl in 3,3-pybz. As a result, the paired

Table 2. Selected bond lengths (Å) and angles (°) for **1** and **2**.

Complex **1**			
Cu(1)–O(2)	1.9480(17)	Cu(1)–O(4)	1.9782(16)
Cu(1)–N(2B)	2.027(2)	Cu(1)–N(1A)	2.035(2)
Cu(1)–O(5)	2.307(2)	N(2)–Cu(1A)	2.027(2)
O(2)–Cu(1)–O(4)	173.65(7)	O(2)–Cu(1)–N(2B)	87.25(8)
O(4)–Cu(1)–N(2B)	90.02(8)	O(2)–Cu(1)–N(1A)	90.74(8)
O(4)–Cu(1)–N(1A)	90.23(7)	N(2B)–Cu(1)–N(1A)	163.26(8)
O(2)–Cu(1)–O(5)	92.93(7)	O(4)–Cu(1)–O(5)	93.17(7)
N(2B)–Cu(1)–O(5)	99.38(8)	N(1A)–Cu(1)–O(5)	97.32(8)
Complex **2**			
Ni(1)–O(4A)	2.0023(14)	Ni(1)–O(5)	2.0574(14)
Ni(1)–N(2)	2.0940(17)	Ni(1)–N(1B)	2.1051(17)
Ni(1)–O(2)	2.1169(14)	Ni(1)–O(1)	2.1786(14)
O(4A)–Ni(1)–O(5)	92.85(6)	O(4A)–Ni(1)–N(2)	90.14(6)
O(5)–Ni(1)–N(2)	88.63(6)	O(4A)–Ni(1)–N(1B)	90.35(7)
O(5)–Ni(1)–N(1B)	176.72(6)	N(2)–Ni(1)–N(1B)	92.07(7)
O(4A)–Ni(1)–O(2)	170.07(6)	O(5)–Ni(1)–O(2)	88.15(6)
N(2)–Ni(1)–O(2)	99.77(6)	N(1B)–Ni(1)–O(2)	88.57(6)
O(4A)–Ni(1)–O(1)	108.89(6)	O(5)–Ni(1)–O(1)	88.92(6)
N(2)–Ni(1)–O(1)	160.91(6)	N(1B)–Ni(1)–O(1)	89.38(6)
O(2)–Ni(1)–O(1)	61.23(5)		

Symmetry operations for **1**: (A) $x-1/2, -y+3/2, z$; (B) $x+1/2, -y+3/2, z$; for **2**: (A) $x+1, y, z$; (B) $-x, y+1/2, -z+3/2$.

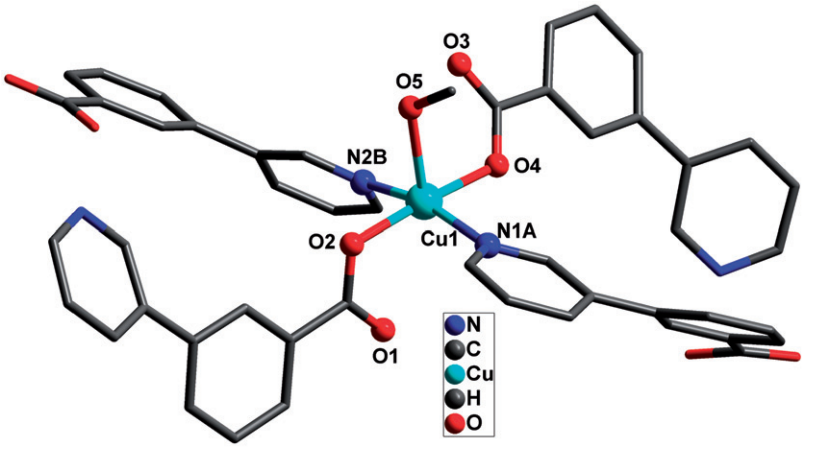

Figure 1. Coordination environment of Cu in **1**. Selected hydrogens are omitted for clarity.

3,3-pybz ligands connect adjacent Cu^{II} ions to generate an infinite 1-D double-strand chain along the *a*-axis, with Cu···Cu separation of 8.354 Å, as shown in figure 2.

3.1.2. Structure of $\{[Ni(3,3\text{-pybz})_2(H_2O)]\cdot(H_2O)\}_n$ (2). The Ni^{II} complex displays a 2-D corrugated framework. Structural analyses reveal two types of 3,3-pybz ligands in the asymmetric unit of **2**, both acting as bidentate bridges to interlink Ni^{II} centers into a 2-D network. One ligand adopts μ_2-unidentate (N_{py})/unidentate(O_{COO^-}) (μ_2-κ_1-N:κ_1-O)

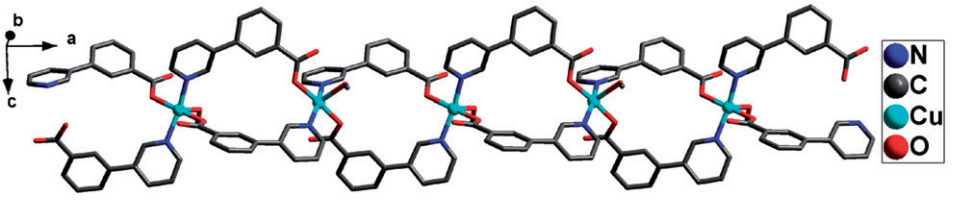

Figure 2. The 1-D double-strand chain of **1** along the *a*-axis.

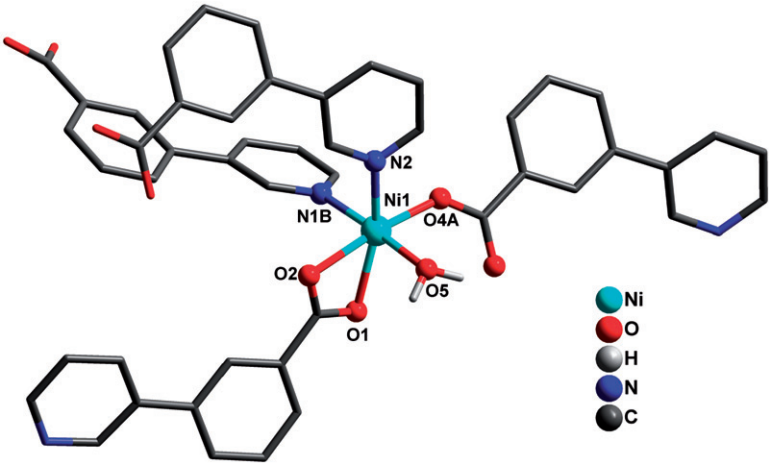

Figure 3. Coordination environment of Ni in **2**. Selected hydrogens are omitted for clarity.

as in **1** while the other takes μ_2-unidentate (N_{py})/bidentate chelating (O_{COO}^-) (μ_2-κ_1-N:κ_2-O see scheme 1B in the Supplementary material). Each Ni^{II} is six-coordinate to four 3,3-pybz ligands *via* two pyridyl-N and three carboxylate-O as well as one water molecule (figure 3), taking a distorted NiO_4N_2 octahedral geometry. The Ni–O bond lengths are 2.0023(14) and 2.1786(14) Å and the Cu–N bond distances are 2.0940(17) and 2.1051(17) Å. The O/N–Ni–O/N bond angles are 87.25(8)° and 173.65(7)°. In **2**, the dihedral angles are 33.07° (μ_2-N, O) and 15.74° (μ_2-N, O, O) between pyridine and phenyl in 3,3-pybz ligand.

Further investigation indicates that the two types of 3,3-pybz ligands link Ni^{II} centers to generate a 2-D corrugated network with a simple (4,4) topology (figure 4). These 2-D layers are embedded into each other and adopt an interdigitated packing, fixed by interlayer hydrogen-bonding between the aqua ligands and the carboxylate oxygen, and strong aromatic π–π stacking interactions between 3,3-pybz ligands. Details are as follows: O5-H25···O1 and O5-H26···O3 for **2** (H···O/O···O distance: 1.945/2.735 Å and 1.825/2.665 Å, angle: 154.27° and 169.26°), π–π stacking interactions between pyridyl rings: (centroid-to-centroid distance 3.712 Å) (figure 5). Furthermore, through strong aromatic π–π stacking interactions and O–H···O hydrogen bonds, those 2-D layers are enlarged to form the final 3-D framework, viewed along the crystallographic *a*-axis (figure 6).

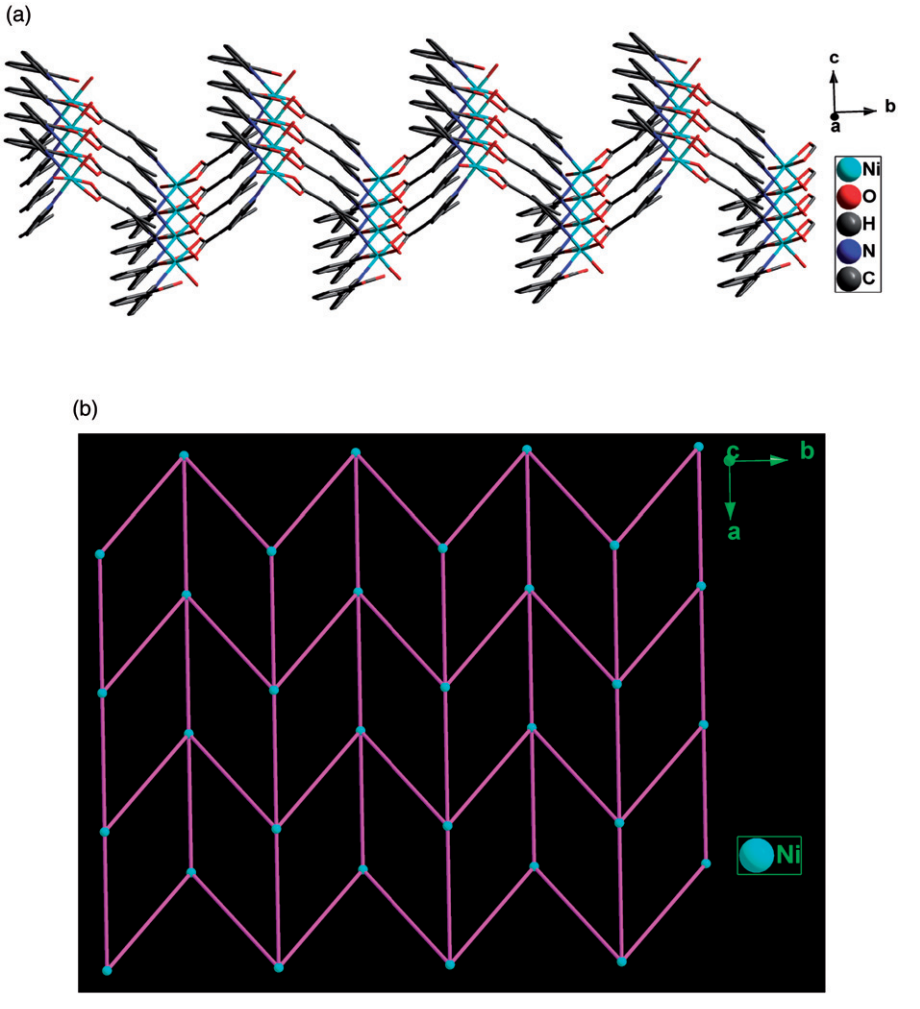

Figure 4. (a) The 2-D corrugated framework in **2** and (b) the schematic diagram of (4,4) sheet viewed along the *c*-axis.

3.2. *Thermogravimetric analysis*

To examine the thermal stabilities of the complexes, TGA were carried out for **1** and **2** between 20°C and 700°C (figures S1 and S2 in the "Supplementary material"). TG curve of **1** exhibits a two-stage weight loss, giving total loss of 88.6% of its initial weight between 50°C and 460°C. The first weight loss is 13.2% from 50°C to 120°C, corresponding to release of one free DMF (Calcd 12.94%). The second weight loss of 75.4% from 280°C to 460°C is attributed to removal of CH_3OH and 3,3-pybz (Calcd 75.82%). TG curve of **2** exhibits weight loss of 7.62% from 100°C to 210°C, corresponding to loss of two water molecules (Calcd 7.34%) and no further weight loss until 350°C, where significant weight loss of 80.4% occurred ending at 520°C, for complete decomposition of 3,3-pybz ligands (Calcd 80.71%).

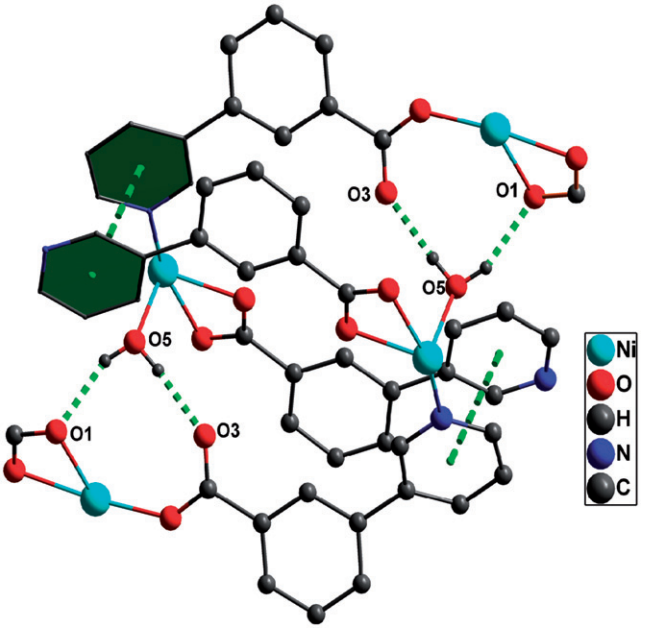

Figure 5. View of the π–π stacking interaction and hydrogen-bonded pattern in **2**.

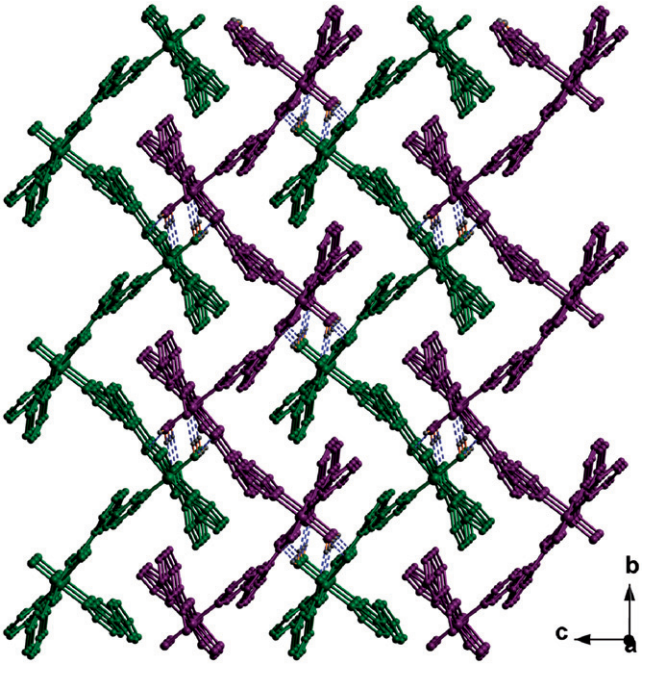

Figure 6. The 3-D hydrogen-bonded net of **2**.

3.3. *IR spectra*

The IR spectra of **1** and **2** exhibit characteristic bands of carboxylate, asymmetric and symmetric stretching at 1602 and 1421 cm^{-1} for **1** and at 1626, 1546 and 1434, 1411 cm^{-1} for **2**. The separation between $v_{asym}(CO_2)$ and $v_{sym}(CO_2)$ indicates that the carboxylates coordinate monodentate (181 cm^{-1} for **1**, 192 cm^{-1} for **2**) and chelating bidentate (135 cm^{-1} for **2**) [20], which is also confirmed by the X-ray analysis.

3.4. *Magnetic properties*

The magnetic properties of **1** and **2** were investigated from 3 to 300 K in a field of 10 kOe. The magnetic susceptibilities χ_M and $\chi_M T$ *versus* T plots are shown in figure 7. For **1**, the experimental $\chi_M T$ value at 300 K is 0.379 $cm^3\,K\,mol^{-1}$, slightly larger than the spin-only value (0.375 $cm^3\,K\,mol^{-1}$) expected for the spin-only Cu(II) ion (figure 7a). As T is lowered, $\chi_M T$ decreases continuously to a value of 0.058 $cm^3\,K\,mol^{-1}$ at 3 K. This behavior indicates a dominant antiferromagnetic interaction between the Cu(II) ions. In **1**, the Cu···Cu distance through the mal bridge is 8.354 Å. The temperature dependence of the reciprocal susceptibilities ($1/\chi_M$) obeys the Curie–Weiss law above 3 K with $\theta = -7.30$ K, $C = 0.387$, and $R = 1.47 \times 10^{-4}$. The values of θ for **1** indicate weak antiferromagnetic interactions between the adjacent Cu(II) ions.

For **2**, the experimental $\chi_M T$ value at 300 K is 2.28 $cm^3\,K\,mol^{-1}$, slightly larger than the spin-only value (2.00 $cm^3\,K\,mol^{-1}$) expected for the spin-only Ni^{II} ion (figure 7b). As T is lowered, the $\chi_M T$ value of **2** decreases continuously to a value of 0.336 $cm^3\,K\,mol^{-1}$ at 3 K, indicating a potential antiferromagnetic interaction between Ni^{II} ions. As indicated by the crystal structure of **2**, the Ni^{II} ions are a 2-D coordination network, and the Ni···Ni distance through the 3,3-pybz bridges are 10.472 Å and 11.443 Å. There are no close-contact 1-D chains (Ni–O–C–O–Ni) in the structure, and the distance across the 3,3-pybz ligands is too great for any real magnetic super-exchange. The explanation for the decrease in $\chi_M T$ product is hydrogen-bonding facilitated super-exchange (Ni–O–H···O–Ni) between nickels in neighboring frameworks (Ni···Ni distance: 5.236 Å) and zero-field splitting (D) due to degeneracy breaking in distorted octahedral environment for the d^8 Ni^{II}. The magnetic data were fit to equation (1), derived for an Heisenberg dimer of $S = 1$ spins [21],

$$\chi_M T = (Ng^2\beta^2/k)\left[(e^x + 5e^{3x})/(1 + e^x + 5e^{3x})\right] + \chi_{TI} T, \quad (1)$$

where $x = J/kT$. Least-squares fitting of the data applying equation (1) leads to $J = -5.48\ cm^{-1}$, $g = 2.03$, $\chi_{TI} = -6.35 \times 10^{-4}\ cm^3\,mol^{-1}$ and $R = 7.35 \times 10^{-4}$ with agreement factor defined as $R = \sum[(\chi_M)_{obs} - (\chi_M)_{calc}]^2/\sum[(\chi_M)_{obs}]^2$. The negative coupling constant J confirms the existence of a weak antiferromagnetic exchange within **2**.

4. Conclusion

By selecting 3-pyridin-3-yl-benzoic acid, we have synthesized and characterized two coordination polymers, $\{[Cu(3,3\text{-pybz})_2(CH_3OH)]\cdot(DMF)\}_n$ (**1**) and $\{[Ni(3,3\text{-pybz})_2(H_2O)]\cdot(H_2O)\}_n$ (**2**). Complex **1** exhibits an infinite 1-D double-strand chain

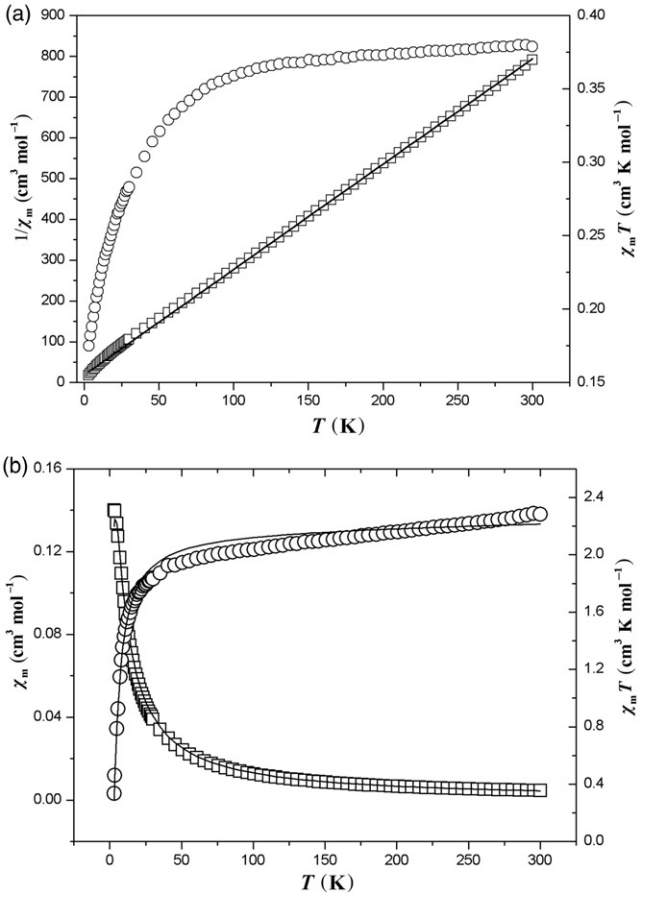

Figure 7. (a) Thermal variation of $1/\chi_M$ and $\chi_M T$ for **1**: □ – $1/\chi_M$ experimental values, ○ – $\chi_M T$ experimental values and (b) thermal variation of χ_M and $\chi_M T$ for **2**: □ – χ_M experimental values, ○ – $\chi_M T$ experimental values.

and **2** displays a 2-D corrugated framework with a simple (4,4) topology; each is further enlarged to form the final 3-D supramolecular structure. Magnetic behavior of **1** and **2** shows antiferromagnetic interactions. These results may provide impetus and insight for crystal engineering of pyridine carboxylate-based complexes with desired structures and useful properties.

Supplementary material

Additional crystallographic data sets for the structures are available through the Cambridge Structural Data Base as supplementary publication reference number CCDC-824635 for **1** and CCDC-824636 for **2**. Copies of this information may be obtained from the Director, CCDC, 12 Union Road, Cambridge, CB21EZ, UK

(Fax: +44 1223 336033; E-mail: deposit@ccdc.cam.ac.uk or www: http://www.ccdc.cam.ac.uk).

Acknowledgments

This work was supported by the Nature Scientific Research Foundation of Shaanxi Provincial Education Office of China (No. 2010JK905).

References

[1] G. Ferey, C. Mellot-Draznieks, C. Serre, F. Millange. *Acc. Chem. Res.*, **38**, 217 (2005).
[2] J.L.C. Rowsell, O.M. Yaghi. *Angew. Chem. Int. Ed.*, **44**, 4670 (2005).
[3] S. Kitagawa, S. Noro, T. Nakamura. *Chem. Commun.*, **45**, 701 (2006).
[4] M.H. Zeng, Q.X. Wang, Y.X. Tan, S. Hu, H.X. Zhao, L.S. Long, M. Kurmoo. *J. Am. Chem. Soc.*, **132**, 2561 (2010).
[5] F. Fu, D.S. Li, C.Q. Zhang, J.J. Wang, Y.P. Wu, M. Du, J.W. Wang. *Inorg. Chem. Commun.*, **11**, 1260 (2008).
[6] Y.B. Zhang, W.X. Zhang, F.Y. Feng, J.P. Zhang, X.M. Chen. *Angew. Chem. Int. Ed.*, **48**, 5287 (2009).
[7] Z.L. Wang, W.H. Fang, G.Y. Yang. *Chem. Commun.*, **46**, 8216 (2010).
[8] R.Q. Zhong, R.Q. Zou, M. Du, L. Jiang, T. Yamada, G. Maruta, S. Takeda, Q. Xu. *CrystEngComm*, **10**, 605 (2008).
[9] X.J. Jiang, M. Du, Y. Sun, J.H. Guo, J.S. Li. *J. Solid State Chem.*, **182**, 3211 (2009).
[10] M.H. Zeng, Y.L. Zhou, M.C. Wu, H.L. Sun, M. Du. *Inorg. Chem.*, **49**, 6436 (2010).
[11] D.S. Li, L. Tang, F. Fu, M. Du, J. Zhao, N. Wang, P. Zhang. *Inorg. Chem. Commun.*, **13**, 1126 (2010).
[12] L. Tang, Y.P. Wu, F. Fu, P. Zhang, N. Wang, L.F. Gao. *J. Coord. Chem.*, **63**, 1873 (2010).
[13] L. Tang, Y.P. Wu, F. Fu, W.L. Wang, Y.Y. Lian, F. Hu, A.M. Bai. *Acta Chim. Sin.*, **68**, 1261 (2010).
[14] L. Tang, F. Fu, L.J. Gao, Y.P. Wu, Q.R. Liu, X.M. Gao. *Z. Anorg. Allg. Chem.*, **637**, 608 (2011).
[15] Y.P. Wu, D.S. Li, F. Fu, L. Tang, J.J. Wang, X.G. Yang. *J. Coord. Chem.*, **62**, 2665 (2009).
[16] R.Q. Zhong, R.Q. Zou, M. Du, L. Jiang, T. Yamada, G. Maruta, S. Takeda, Q. Xu. *CrystEngComm*, **10**, 605 (2008).
[17] F. Guo. *J. Coord. Chem.*, **62**, 3606 (2009).
[18] G.M. Sheldrick. *SHELXS 97, Program for Crystal Structure Solution*, University of Göttingen, Germany (1997).
[19] G.M. Sheldrick. *SHELXL 97, Program for the Refinement of Crystal Structures*, University of Göttingen, Germany (1997).
[20] Y.P. Wu, D.S. Li, F. Fu, W.W. Dong, L. Tang, Y.Y. Wang. *Inorg. Chem. Commun.*, **13**, 1005 (2010).
[21] B. Bleaney, K.D. Bowers. *Proc. R. Soc. London, Ser. A*, **214**, 451 (1952).